ARTICLES SCIENCE CHINA Materials

mater.scichina.com link.springer.com

Published online 29 August 2019 | https://doi.org/10.1007/s40843-019-9555-0

Sci China Mater 2020, 63(1): 62–74

Facile microwave approach towards high performance MoS_2/graphene nanocomposite for hydrogen evolution reaction

Shatila Sarwar[1], Amit Nautiyal[1], Jonathan Cook[1], Yifei Yuan[2,3], Junhao Li[4], Sunil Uprety[4], Reza Shahbazian-Yassar[2], Ruigang Wang[4], Minseo Park[5], Michael J. Bozack[5] and Xinyu Zhang[1*]

ABSTRACT **Low-cost, highly efficient catalysts for hydrogen evolution reaction (HER) are very important to advance energy economy based on clean hydrogen gas. Intensive studies on two-dimensional molybdenum disulfides (2D MoS_2) have been conducted due to their remarkable catalytic properties. However, most of the reported syntheses are time consuming, complicated and less efficient. The present work demonstrates the production of MoS_2/graphene catalyst *via* an ultra-fast (60 s) microwave-initiated approach. High specific surface area and conductivity of graphene delivers a favorable conductive network for the growth of MoS_2 nanosheets, along with rapid charge transfer kinetics. As-produced MoS_2/graphene nanocomposites exhibit superior electrocatalytic activity for the HER in acidic medium, with a low onset potential of 62 mV, high cathodic currents and a Tafel slope of 43.3 mV/decade. Beyond excellent catalytic activity, MoS_2/graphene reveals long cycling stability with a very high cathodic current density of around 1000 mA cm^{-2} at an overpotential of 250 mV. Moreover, the MoS_2/graphene-catalyst exhibits outstanding HER activities in a temperature range of 30 to 120°C with low activation energy of 36.51 kJ mol^{-1}, providing the opportunity of practical scalable processing.**

Keywords: microwave-initiated synthesis, MoS_2/graphene nanocomposite, electrocatalysis, hydrogen evolution reaction

INTRODUCTION

Because of present climate issues and the deterioration of existing natural resources, the energy dependency on fossil fuels is becoming disputed in many ways. To resolve this energy crisis, hydrogen is considered as a promising energy carrier for clean and sustainable energy technologies, especially for the intermittent renewable resources such as solar, hydro or wind energy [1–3]. Though water electrolysis is solely the green approach to generate hydrogen energy, large-scale hydrogen production through photo/electrolysis is still very challenging due to the lack of energy-efficient and cost-effective techniques. The electrolysis process requires advanced electrocatalyst to reduce the overpotential and accelerate the kinetically rate-limiting steps involved within reductive half reaction of water splitting, known as the hydrogen evolution reaction (HER, i.e., $2H^+ + 2e^- \rightarrow H_2$) [1,4]. To date, platinum (Pt) and its composites are known to be the most effective HER electrocatalysts in acidic media. However, the high cost and low earth abundance of these materials severely hinder their commercial applications. Nonprecious catalysts, which are made from earth-abundant elements are therefore emerging for a large-scale implementation as HER catalysts [5,6]. To develop the cost-effective alternatives to Pt, intense research is being conducted for hydrogen production through photo/electrocatalytic method. Such alternatives typically include nickel or nickel-based materials, which operate in alkaline electrolytes [7–9]. Nevertheless, HER generally requires acidic conditions and the long-term stability of low-cost catalysts needs to be improved in acidic electrolytes. Inspired by the HER mechanisms of natural catalysts such as hydrogenase and nitrogenase enzymes, metal chalcogenides

[1] Department of Chemical Engineering, Auburn University, Auburn, AL 36849, USA
[2] Department of Mechanical and Industrial Engineering, University of Illinois at Chicago, Chicago, IL 60607, USA
[3] Chemical Sciences and Engineering Division, Argonne National Laboratory, IL, 60439, USA
[4] Department of Metallurgical and Materials Engineering, University of Alabama, Tuscaloosa, AL 35487, USA
[5] Department of Physics, Auburn University, Auburn, AL 36849, USA
* Corresponding author (email: xzz0004@auburn.edu)

(MCs) containing non-noble metals (Mo, W or Co) have been designed to catalyze the electrochemical production of hydrogen [10,11]. Among all the MCs, molybdenum disulfide (MoS_2) and its compounds have recently emerged as a very promising class of nonprecious, earth-abundant HER catalyst with high catalytic activity and good stability in acidic electrolytes [12–15]. In comparison to bulk MoS_2, nanocrystallized MoS_2 has been identified as a promising catalyst because of more active edges in the nanostructured forms. In the past few years, extensive effort has been devoted to improving the HER catalytic activity of MoS_2 by identifying and exposing active sites [16,17], as well as enhancing electron transport through nanostructuring, shape controlling, phase engineering, doping, intercalation, hybridization, and so on [12,16,18–23]. Besides morphology, the electrical conductivity is another key factor that influences the electrocatalytic efficiency of HER catalysts. Taking these factors into account, carbon materials such as conducting polymers, graphene, reduced graphene oxide (r-GO), carbon nanotubes (CNTs), etc. are considered as ideal supports to improve the electrocatalytic activity because of their unique properties. The honeycomb graphene structure, which consists of extended two-dimensional (2D) sheets of sp^2-bonded carbon atoms, shows superior properties, such as fast mobility of charge carriers, high electrical conductivity and exceptionally large specific surface area [24,25]. Therefore, various forms of graphene have been investigated as potential conducting supports for MoS_2 catalyst to demonstrate high HER electrocatalytic activity [18,26,27]. To synthesize these hybrid materials, most of the approaches require complex equipment setups, long processing time, high energy consumption, along with safety, scalability and cost issues which limit the range of potential applications. Several examples involve the use of toxic gases along with calcination under H_2/Ar atmosphere [28], long-time heating of precursor materials [29], complex lyophilization dehydration process [30], cumbersome electro-deposition which requires advanced care [31], and so on. In this regard, microwave-initiated manufacturing may be a promising approach to develop efficient MoS_2/graphene-catalyst for HER. In present, the application of microwave approach in synthetic chemistry is a fast-growing research area, due to its advantages such as faster volumetric heating, higher reaction rate, higher selectivity, reduced reaction time, and increased yields of products compared with conventional heating methods [32–34]. Successful synthesis of MCs by microwave-initiated approach has been reported and demonstrated that it can be used for the highly efficient production of different hybrid compounds [35–38].

In this work, we demonstrated the direct growth of a nanocomposite of MoS_2 on graphene substrate *via* a facile, scalable and efficient microwave-initiated approach (Scheme 1), following the previous study of our group to synthesize MCs on polypyrrole nanofiber substrate [38]. This technique represents a clean, ultrafast (60 s) synthetic approach using microwave heating without any inert gas protection or use of intense facilities. More importantly, graphene exhibits strong interaction with microwaves making it an efficient susceptor to achieve microwave-heating rapidly and uniformly. During the reaction, the strong interaction between substrate mate-

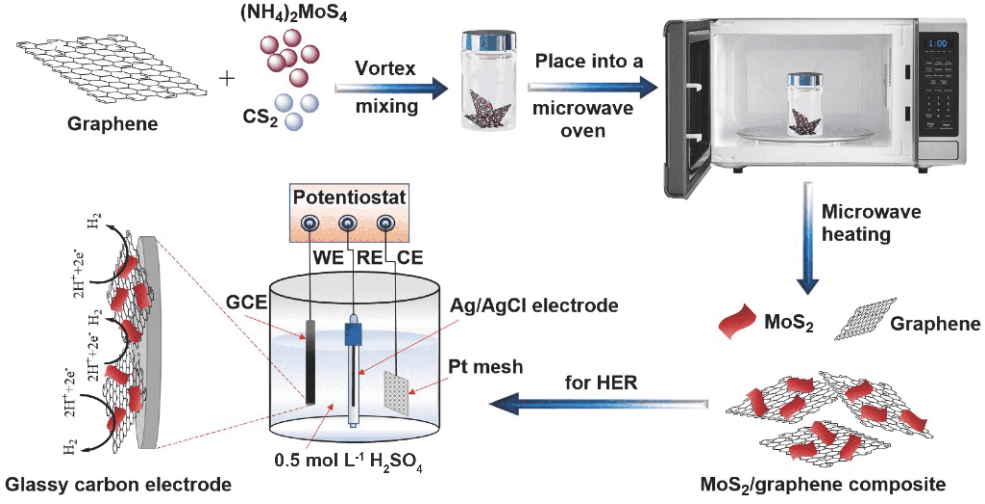

Scheme 1 Illustration of the microwave-initiated synthesis of MoS_2/graphene composite, employed as an electrocatalyst for HER.

rial and microwave-irradiation takes place to achieve fast thermal decomposition of molybdenum-containing precursor to synthesize uniformly dispersed MoS_2/graphene nanocomposites. Benefiting from the synergistic effects of MoS_2 catalyst and graphene, this MoS_2/graphene nanocomposite has been demonstrated to be an active non-precious metal-based catalyst for HER. As-produced MoS_2/graphene-catalyst exhibited low overpotential, small Tafel slope with a very high cathodic current density, along with fascinating cycling activation behavior and high stability under acidic condition, even at high operating temperatures (30–120°C).

EXPERIMENTAL

Materials and reagents

Ammonium tetrathiomolybdate ($(NH_4)_2MoS_4$, 99.95%) was purchased from BeanTown Chemical, Inc. Carbon disulfide (CS_2, liquid, 99.9%), molybdenum(IV) sulfide (MoS_2, ~325 mesh powder, 98%), and poly(vinylidene fluoride) (PVDF powder, $(-CH_2CF_2-)_n$) were purchased from Alfa Aesar. *N*,*N*-dimethylformamide ($HCON(CH_3)_2$, DMF) was obtained from Macron Fine Chemicals™. Nitric acid (69%–70%), and acetone (CH_3COCH_3) were supplied by BDH Chemicals, VWR. Graphene substrate was obtained from Magnolia Ridge Inc. Sulfuric acid was purchased from Anachemia. All chemicals purchased were used without further treatment or purification. For electrochemical characterizations, Pt gauze (100 mesh, 99.9% metal basis) was obtained from Alfa Aesar. Glassy carbon electrode (CHI 104, 3 mm in diameter) was purchased from CH Instruments, Inc. and silver/silver chloride (Ag/AgCl, 3 mol L^{-1} KCl, E^o= +0.197 V *vs.* reversible hydrogen electrode (RHE)) electrode was acquired from Hach.

Microwave-initiated synthesis of MoS_2/graphene nanocomposites

MoS_2/graphene compound was prepared by the reaction of ammonium tetrathiomolybdate (ATTM) and CS_2 on graphene substrate using microwave-initiated synthesis method. Equal amounts (15 mg each) of ATTM and graphene were taken in a glass vial and mixed together homogeneously by a speed mixer at 2000 rpm. After a while, CS_2 solvent (200 μL) was added and mixed well by speed mixer at 2000 rpm. The solvent was evaporated after 10 min of air drying. Next, the uniform blend of dried ATTM-graphene-CS_2 was subjected to microwave irradiation in a domestic microwave oven (frequency 2.45 GHz, power 1250 W) for 60 s. Graphene served as a substrate to absorb the microwave energy and convert it to heat energy. During the process, microwave heating triggered the reduction of ATTM to MoO_2, and then converted to MoS_2 dispersed on graphene substrate, releasing other constituents in gaseous forms. Thus, the synthesis of MoS_2/graphene nanocomposite took place for 60 s under microwave irradiation.

Characterizations

The surface morphologies and chemical compositions of graphene and MoS_2/graphene were characterized by scanning electron microscope (SEM; JEOL 7000 FE), coupled with an energy dispersive X-ray spectrometer (EDS, Oxford Instruments) with an acceleration voltage of 20 kV. The transmission electron microscopy (TEM), high resolution TEM (HRTEM) and selected area electron diffraction (SAED) experiments were carried out using JEOL JEM-3010 TEM with a LaB6 electron gun operated under 300 kV. Micro-Raman spectroscopy was performed on the samples at room temperature by employing back-scattering geometry using the 442 nm line (80 mW) of a dual wavelength He-Cd laser (Kimmon Electric). The X-ray diffraction (XRD) patterns of MoS_2/graphene were analyzed by a Bruker D8 Advance X-ray powder diffractometer with Ni filtered CuKα radiation (wavelength, λ=1.5406 Å). Photoemission measurements were performed in a load-locked Kratos XSAM 800 surface analysis system and X-ray photoelectron spectroscopy (XPS) spectra were recorded in the fixed analyzer transmission (FAT) mode with a pass energy of 80 eV. In addition, nitrogen adsorption isotherms were measured with the aid of Quantachrome's Nova 2200e instrument at 77 K. The Brunauer-Emmett-Teller (BET) method was used to calculate the specific surface area.

Electrochemical measurements

Before each electrochemical experiment, glassy carbon electrode (GCE) was polished with alumina powder (Al_2O_3, 0.05 μm) on a polishing mat to obtain a mirror-finished surface, followed by immersing in 6 mol L^{-1} HNO_3 for 10 min, rinsing with deionized (DI) water and vacuum drying. To prepare the working electrode, MoS_2/graphene hybrid catalyst (2 mg) was mixed with PVDF powder (0.2 mg) and DMF (50 μL) to form a homogeneous black slurry. The catalyst slurry was drop-coated onto the clean surface of GCE (0.07 cm^2) with a mass loading of ~5 mg cm^{-2}, which was then dried in a vacuum dryer at 60°C for 30 min. For comparison, GCEs were also coated with pure MoS_2, pure graphene, and a physical mixture of MoS_2 and graphene (MoS_2+graphene)

following the same steps. All electrochemical studies were performed using a CH Instrument (CHI 760D) potentiostat using 'Electrochemical Analyzer' software (version 15.03) in a standard three-electrode setup consisting of a glassy carbon working electrode, silver chloride electrode (Ag/AgCl, 3 mol L^{-1} KCl) as the reference, and Pt mesh as a counter electrode in 0.5 mol L^{-1} H_2SO_4 electrolyte. To determine the HER activities of samples, the potentials were referred to the RHE by using the equation: V (*vs.* RHE) = V (*vs.* Ag/AgCl) + 0.197 + (0.059 × pH). The electrocatalytic activity of MoS_2/graphene towards HER was examined by polarization curves using linear sweep voltammetry (LSV) at a scan rate of 1 mV s^{-1} in 0.5 mol L^{-1} H_2SO_4 at room temperature. Before each LSV measurement, cyclic voltammetry (CV) was run for 50 cycles to achieve stable condition. CV was also performed to determine active surface area of catalyst samples. Prior to each measurement of LSV and CV, a resistance test was made and the *iR* compensation was applied using the CHI software. Electrochemical impedance spectroscopic (EIS) measurements were carried out in 0.5 mol L^{-1} H_2SO_4 at various overpotentials from 50 to 300 mV (*vs.* RHE) in the frequency range of 10^{-2} to 10^6 Hz with a single modulated alternating current (AC) potential of 5 mV. Afterward, the EIS spectra were fitted by the EC-Lab software.

RESULTS & DISCUSSION

As-produced MoS_2/graphene composite was analyzed by physical characterizations to confirm the successful synthesis of MoS_2 nanosheets on graphene substrate, as well as for morphologies and microstructural analyses. Furthermore, several electrochemical characterizations were performed to obtain the enhanced catalytic activities of MoS_2/graphene toward HER.

Material characterizations

The surface morphologies of pure graphene and MoS_2/graphene were investigated by SEM. As shown in Fig. 1a, b, graphene shows thick flake-like structures. Whereas after microwave-initiated synthesis, the MoS_2 layers (Fig. 1c, d) were embedded in graphene flakes, substantiating the successful synthesis of MoS_2/graphene nanocomposite. HRTEM imaging was performed to examine the microstructure and crystallinity of MoS_2/graphene nanocomposite (Fig. 1e, f), displaying the difference between graphene and MoS_2 nanosheets. The MoS_2 exhibits the few-layered structure with an interlayer distance of 6.4 Å, while the graphene shows 3.75 Å interlayer distance. MoS_2 nanosheets demonstrate the corrugated layers in the low-magnification TEM image, as shown in Fig. 1g. In addition, the SAED pattern of corresponding area (marked as 'area 1' in Fig. 1g, h) displays broad and hazy diffraction rings, which indicates low crystallization of MoS_2 on crystal graphene surface.

The EDS results reveal (Fig. 2a) that the nanosheets are primarily composed of molybdenum (Mo) and sulfur (S). Additionally, a huge amount (~80 wt%) of carbon (C) was found due to the graphene substrate. The atomic ratio of Mo and S is very close to 1:2, confirming the formation of MoS_2 in the as-produced nanocomposites. Furthermore, Raman spectra of pure graphene and MoS_2/graphene are shown in Fig. 2b, c. The characteristic Raman peaks for graphene (D, G and 2D bands) are clear and in the MoS_2/graphene peaks, the composite is crystalline 2H–MoS_2, confirmed by the Raman peaks located

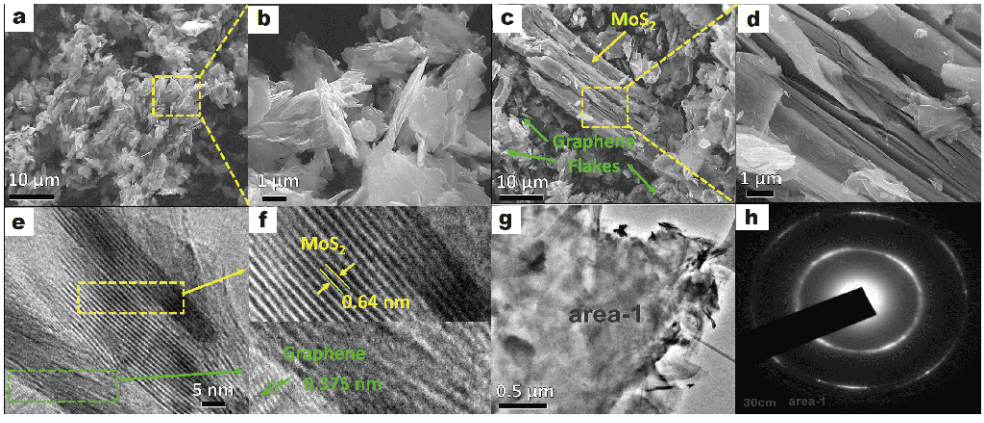

Figure 1 SEM images of (a, b) graphene flakes and (c, d) layered MoS_2 embedded in graphene, at low and high magnifications. (e) HRTEM image of MoS_2/graphene. (f) High-magnification HRTEM image of MoS_2 nanosheets and graphene. The interlayer distance of MoS_2 nanosheets is around 6.4 Å. (g) Low-magnification TEM image of MoS_2/graphene nanocomposite. (h) SAED pattern of MoS_2 nanosheets.

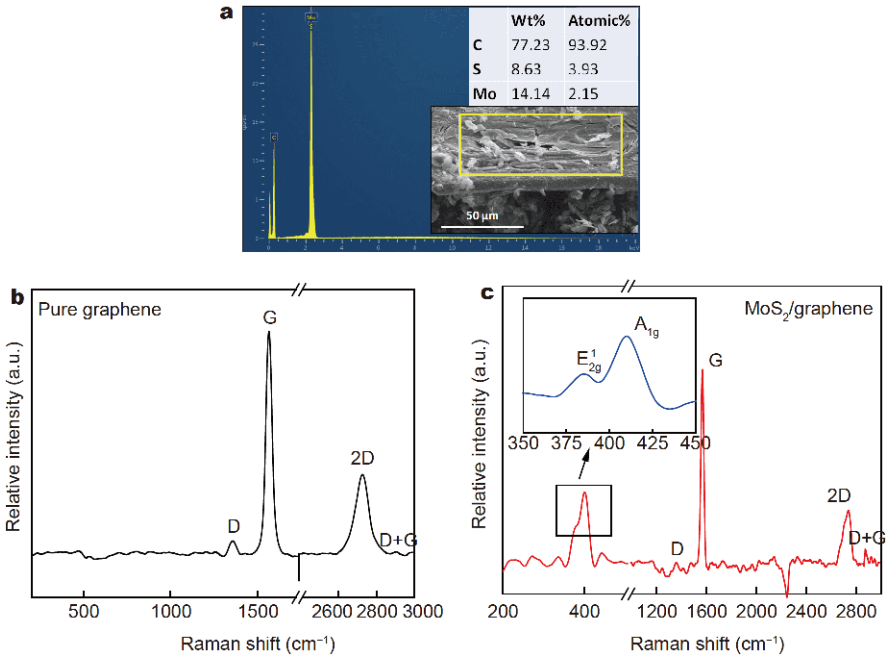

Figure 2 (a) EDS pattern of MoS_2/graphene nanocomposite (inset table: wt% and at% of carbon (C), sulfur (S), and molybdenum (Mo). Raman spectra of (b) pure graphene and (c) MoS_2/graphene composite (inset: MoS_2 peaks).

at 384.9 cm^{-1} (in-plane E^1_{2g} mode) and 409.3 cm^{-1} (out-of-plane A_{1g} mode) [39,40]. Previously, it has been reported that the energy difference between two Raman peaks (Δ) can be used to detect the number of MoS_2 layers [39,41]. In this work, Δ is about 24.4 cm^{-1}, indicating the existence of the five to six layered MoS_2 nanosheets.

Furthermore, XRD and XPS analyses were performed to identify the formation of crystalline MoS_2 nanosheets. The XRD pattern of the MoS_2 (Fig. 3a) displays diffraction peaks in the range from 10° to 70°. The peaks at 14.2°, 33.5°, 39.8°, 43.1°, 49.1° and 59.3° are corresponding to (002), (100), (103), (006), (105) and (110) planes, respectively, indexed to the standard hexagonal 2H–MoS_2 structure (JPCDS No. 37-1492) [42], indicating that after reacting under microwave irradiation Mo-precursor with CS_2 solution completely reduce to MoS_2. With almost 80 wt% graphene, the MoS_2/graphene composite displays a peak at ~26° with high intensity as a reflection from carbon layers (002) [43]. The peak around 18° could be indexed to (003) plane, suggesting that some of the graphene inset in the van der Waals gap of MoS_2 layers, leading to an expansion of the interplanar spacing [44]. XPS was analyzed to further confirm the microwave reduction of Mo(VI) in $(NH_4)_2MoS_4$ precursor to Mo(IV) in MoS_2. The survey spectrum is represented in Fig. 3b for MoS_2/graphene, showing the peaks for C, Mo, S, and O. The high-resolution XPS spectrum for Mo 3d (Fig. 3c) shows the binding energies of Mo $3d^{5/2}$ and Mo $3d^{3/2}$ peaks at 229.4 and 232.7 eV, respectively, which match with the typical values for Mo(IV) in MoS_2. The peaks at 162.1 and 164.2 eV in Fig. 3d are attributed to $2p^{1/2}$ and $2p^{2/3}$ of S^{2-}. The binding energies observed from this study are close to the previously reported values for MoS_2 [27,30], which further signifies the formation of MoS_2 in the as-produced nanocomposite. In addition, the BET analyses were performed to measure the specific surface areas of pure MoS_2, and MoS_2/graphene nanocomposite, which were found as 3.35 and 28.30 $m^2\ g^{-1}$ (see Supplementary information Fig. S1a, b), respectively. Comparing the BET values of pure MoS_2 and MoS_2/graphene nanocomposite, the graphene support clearly increases the surface area of the nanocomposite. Moreover, to get better catalytic activities for HER, higher surface areas are preferred which can maximize the number of possible reaction sites while minimizing the total volume of the catalyst.

HER activities of MoS_2/graphene nanocomposite

The electrocatalytic HER activities of MoS_2/graphene were investigated in 0.5 mol L^{-1} H_2SO_4 solution by LSV at room temperature, with a scan rate of 1 mV s^{-1} using a

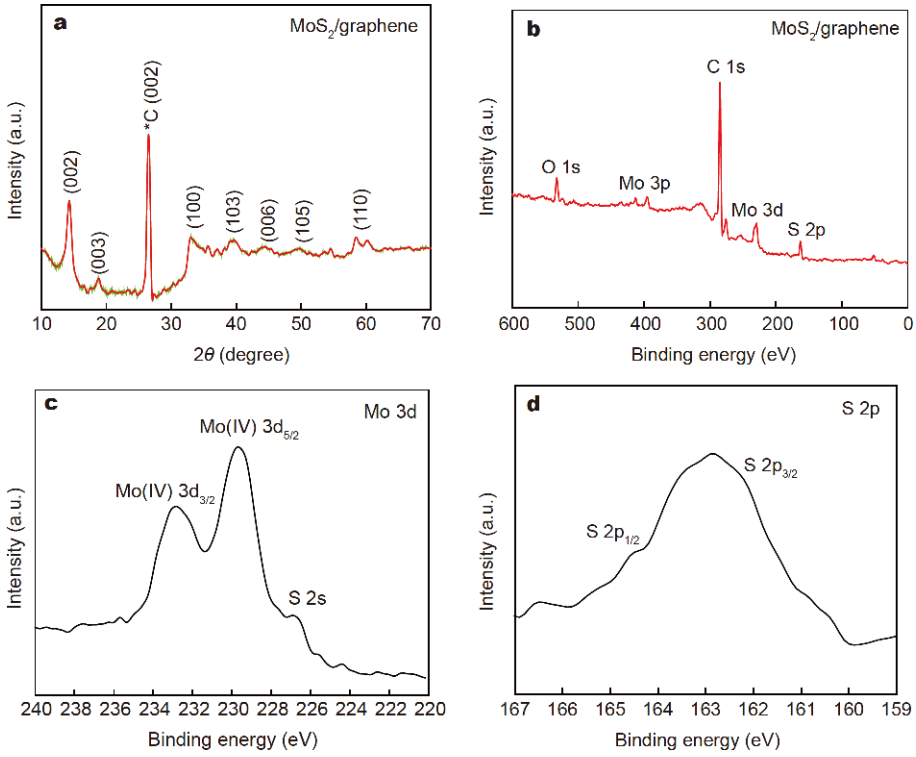

Figure 3 (a) XRD pattern, and (b) XPS spectrum of MoS_2/graphene composite. High resolution XPS spectra of (c) Mo 3d, and (d) S 2p of MoS_2/graphene.

typical three-electrode setup. The pure MoS_2 particles, pure graphene, a physical mixture of MoS_2 and graphene (MoS_2+graphene), commercial Pt catalyst and bare GCE were also studied under the same conditions for comparison. The GCE was coated with catalyst loading of around 5 mg cm^{-2} for each of the electrochemical test. The LSV (*iR* corrected) recorded on MoS_2/graphene shows a small onset potential of 100 mV (Fig. 4a), beyond which the cathodic current increases abruptly when the potential turns more negative. All the major electrochemical parameters are shown in Table 1, which shows the overpotentials (η) for Pt and MoS_2/graphene to reach the current density of 10 mA cm^{-2} are 53 and 183 mV, respectively. In contrast, pure MoS_2 and MoS_2+graphene mixture display trivial HER catalytic activities, while bare GCE and graphene show no catalytic activity with the absence of MoS_2 catalyst (Fig. 4a). To further demonstrate the HER activities, Tafel plots were derived from LSVs by fitting the linear regions to Tafel equation ($\eta = b\log i + a$; where η is the overpotential, b is the Tafel slope, i is the current density and a is a constant). Tafel slope is an inherent property of the catalyst, related to the electrocatalytic reaction mechanism. Theoretically, there are three principal steps for HER in acidic electrolytes, which can elucidate electron transfer kinetics of the catalysts [45,46]. Three possible reactions are given in Equations (1–3):

$$\text{Volmer: } H_3O^+(aq) + e^- + \rightleftharpoons H^* + H_2O(l), \quad (1)$$

$$\text{Heyrovsky: } H^* + H_3O^+(aq) + e^- \rightleftharpoons H_2(g) + H_2O(l) + {}^*, \quad (2)$$

$$\text{Tafel: } H^* + H^* \rightleftharpoons H_2(g) + 2^*. \quad (3)$$

In the above equations, * indicates an empty active site and H^* is a hydrogen atom bound to an active site of catalyst material. The overall HER reaction proceeds through a discharge step (Volmer reaction, Equation (1)) with a Tafel slope around 120 mV/decade, followed by either a desorption step (Heyrovsky reaction, Equation (2)) or recombination step (Tafel reaction, Equation (3)), with the Tafel slopes around 40 and 30 mV per decade, respectively [47]. In this study, MoS_2/graphene exhibits the Tafel slope of 43.3 mV/decade (Fig. 4b), indicating that the Volmer–Heyrovsky reaction mechanism dominates in the HER process of MoS_2/graphene catalyst and the electrochemical desorption is the rate determining step. This high performance of MoS_2/graphene demonstrates the advantage of synergistic effect between MoS_2 nanosheets and graphene, which generates more active

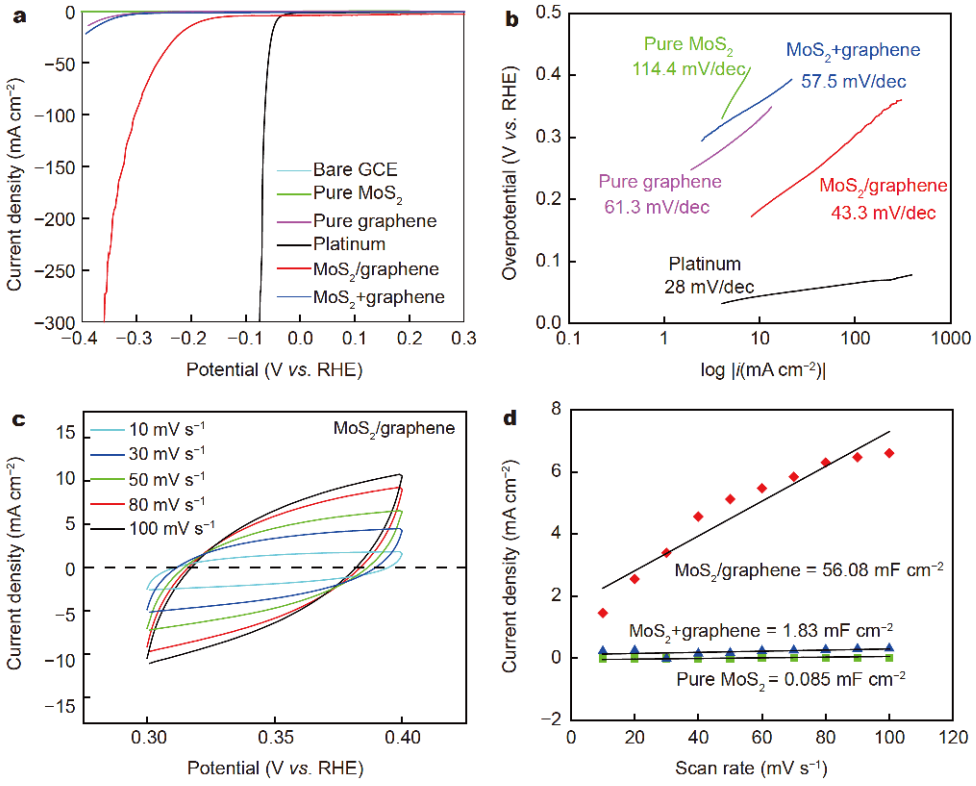

Figure 4 Electrochemical performance of the HER catalysts in 0.5 mol L^{-1} H_2SO_4 with a catalyst load of ~5 mg cm^{-2}: (a) LSVs at a scan rate of 1 mV s^{-1} for bare GCE, pure MoS_2, pure graphene, MoS_2+graphene mixture, MoS_2/graphene composite, and Pt catalyst. (b) Corresponding Tafel plots, showing the Tafel slopes. Electrochemical capacitance measurements: (c) CVs of MoS_2/graphene in a potential window without faradaic reaction; (d) average capacitive current densities at different scan rates for MoS_2/graphene composite, MoS_2+graphene mixture and pure MoS_2.

Table 1 Electrochemical parameters of MoS_2/graphene nanocomposite, comparing with commercial Pt, MoS_2+graphene mixture, pure MoS_2, and pure graphene samples

Samples	Onset potential, η_0 (mV *vs.* RHE)	Over potential, η_{10} (mV *vs.* RHE)	Tafel slope (mV/decade)	Exchange current density, i_0 (mA cm^{-2})
Platinum	45	53	28	3.981
MoS_2/graphene	**100**	**183**	**43.3**	**2.512**
MoS_2+graphene	201	365	57.5	1.007
Pure MoS_2	293	> 400	114.4	-
Pure graphene	204	374	61.3	-

sites for hydrogen evolution. Previous reports show that the exchange current density (i_0) is proportional to the active surface area of catalyst materials, which can be obtained by an extrapolation method (see Fig. S2) on the basis of Tafel equation [48,49]. The i_0 of MoS_2/graphene catalyst was calculated to be 2.512 mA cm^{-2}, very close to the i_0 of commercial Pt (3.981 mA cm^{-2}) (Table 1).

This speculation was further confirmed by the measurement of electrochemical double-layer capacitance (C_{dl}) at solid-liquid interface, another approach to estimate the electrochemically active surface area (ECSA). The ECSA gives an estimation of active reaction sites, which is proportional to C_{dl} [48,50]. To determine C_{dl} values, CV measurements were conducted for MoS_2/graphene catalyst within a potential range (0.3–0.4 V *vs.* RHE) with no apparent faradaic process (Fig. 4c), where the currents were mainly attributed to the charging of the double layer. The double-layer charging current (i_c) is equal to the product of the scan rate (v) and C_{dl}, which can be shown as $i_c = vC_{dl}$ [50]. From this equation, C_{dl} can

be measured from the slope by plotting a straight line of i_c *vs.* v. Representative plots for the determination of active surface areas of MoS_2/graphene, MoS_2+graphene mixture, and pure MoS_2 catalysts are shown in Fig. 4d and Figs S3–S5. The capacitance of MoS_2/graphene was calculated to be 56.08 mF cm^{-2}, whereas those of MoS_2 +graphene and MoS_2 were only 1.83 and 0.085 mF cm^{-2}, respectively. The measured capacitance (C_{dl}) of MoS_2/graphene composite is higher than the previously reported values for MoS_2 compounds, further confirming high catalytic performance [27,30].

Previously reported onset potentials (η_0) and Tafel slopes of molybdenum (Mo-) compounds were compared with the present data of MoS_2/graphene composite in Table 2. In contrast with ultrafast, facile microwave-initiated synthesis performed in this study, previously reported Mo- compounds were synthesized by different complex approaches. Moreover, it is obvious that the present material exhibits low onset potential and a small Tafel slope, that are comparable to other similar compounds. The improved electrocatalytic activity of MoS_2/graphene may be attributed to strong chemical and electronic coupling between MoS_2 nanosheets and graphene, resulting in fast electronic kinetics between the catalyst and electrode surface. This hypothesis was further confirmed by EIS measurements in 0.5 mol L^{-1} H_2SO_4. The electrical equivalent circuit diagram in Fig. 5a was used to model the solid liquid interface, where the constant phase element (CPE) was associated to electrical double layer formed at electrode/electrolyte interface of MoS_2/graphene catalyst. As shown in Fig. 5b, the MoS_2/graphene displays much lower impedance than pure MoS_2 particles and MoS_2+graphene mixture. The charge transfer resistance R_{ct} is related to the kinetics of electrocatalysis and a lower value resembles to a faster reaction rate. Because of the highly conductive surface and strong hydrogen adsorption capacity, MoS_2/graphene catalyst shows a R_{ct} of 1.50 kΩ at overpotential of 180 mV, while pure MoS_2 and MoS_2+graphene mixture present very large R_{ct} of 37.7 and 246.4 kΩ, respectively (Fig. 5b). The solution resistance (R_s) for MoS_2/graphene is 5 Ω, while pure MoS_2 and MoS_2+graphene show higher values of 234.1 and 11.84 Ω, respectively. Hence, much faster electron transfer between the catalytic edge sites of MoS_2/graphene and the electrode surface is one of the key factors contributing to the superior HER kinetics in acidic electrolyte. Additionally, Fig. 5c represents the Nyquist plots of MoS_2/graphene catalyst at various overpotentials of 50−300 mV. In the high frequency zone, the MoS_2/graphene exhibits one capacitive semicircle, indicating that the reaction is kinetically controlled. In this system, R_{ct} decreases significantly with increasing overpotentials, from 7.4 kΩ at 50 mV to only 204.5 Ω at 300 mV (Fig. 5d). Lower R_{ct} illustrated the superior electrocatalytic activity at higher overpotential.

Besides high catalytic activities, good stability towards HER is also a key parameter for practical applications. To investigate the durability under an acidic environment, long-term stability of MoS_2/graphene was tested by CV from 0 to −350 mV *vs.* RHE scanning for 4000 cycles at a scan rate of 50 mV s^{-1} (Fig. 6a). Very interestingly, the catalytic performance of MoS_2/graphene nanocomposite enhances with the potential cycling by reaching the overpotential of only 62 mV after 4000 cycles (see Fig. S6), which is very close to the overpotential (53 mV) of Pt catalyst. Similar improvement in the catalytic performance of MoS_2 by electrochemical cycling has been reported previously [53,54]. The improved catalytic performance during the potential cycling is due to catalytic activation by proton intercalation in MoS_2-layers. Another reason could be the self-optimizing morphological changes by perforation of H_2 bubbles, generating thinner and more porous catalyst materials. To compare the performances, cyclic stabilities of pure MoS_2 and the physical mixture of MoS_2+graphene were conducted (see Figs S7 and S8). As shown in Fig. S7a, pure MoS_2 does not

Table 2 Comparison of electrochemical activities of microwave-synthesized MoS_2/graphene with previously reported MoS_2-graphene compounds

Material	Onset potential (mV *vs.* RHE)	Tafel slope (mV/decade)	Synthesis approach	Ref.
GA-MoS_2	100	41	Hydrothermal	[30]
MoS_2/MGF	100	42	Solvothermal	[51]
MoS_2/RGO	100	41	Solvothermal	[18]
MoS_2/GO-CNT	35	38	Wet-chemical strategy	[43]
MoS_2/RGO_2	140	41	Solvothermal	[52]
MoS_2/graphene	**100**	**43.3**	**Microwave irradiation**	**Present study**

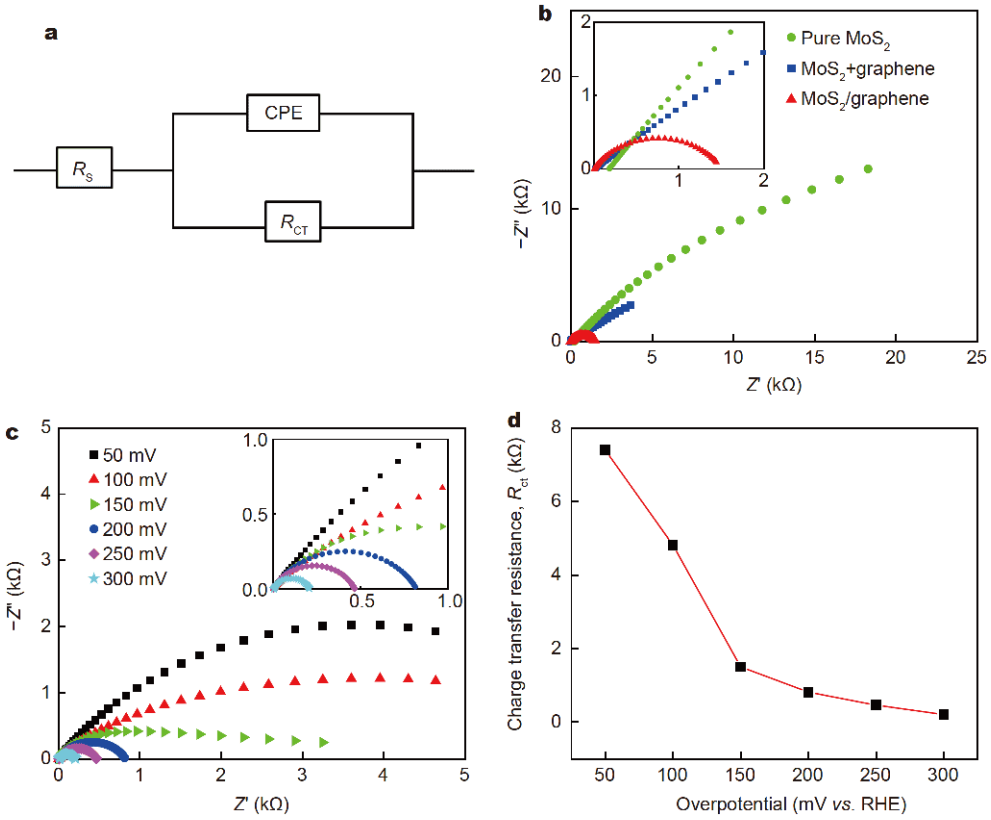

Figure 5 EIS tests: (a) equivalent electrical circuit used to model the HER process on all catalyst samples; (b) EIS of pure MoS_2, physical mixture of MoS_2+graphene, and MoS_2/graphene nanocomposite at an overpotential of 180 mV; (c) Nyquist plots showing the EIS responses of MoS_2/graphene at different overpotentials (50–300 mV) in 0.5 mol L^{-1} H_2SO_4; (d) R_{ct} as a function of HER overpotentials for MoS_2/graphene catalyst.

show any catalytic activity while the physical mixture of MoS_2+graphene (Fig. S7b) exhibits a slight activation, reaching the current density around −50 mA cm^{-2} with an overpotential of around 250 mV *vs.* RHE. These results clearly indicate that the as-produced MoS_2/graphene catalyst possesses the best catalytic behaviors during cyclic stability. Besides cycling stability, the practical operation of as-produced MoS_2/graphene catalyst was examined by electrolysis at constant potential over extended periods. As shown in Fig. 6b, the MoS_2/graphene catalyst shows a stable increase in current density from −140 to −210 mA cm^{-2} for electrolysis over 90 h at a constant overpotential of 180 mV. The increase in current density supports the hypothesis of catalytic activation during the cycling stability. Furthermore, the C_{dl} was calculated for MoS_2/graphene based on CV measurements (Fig. 6c) after 4000 cycles. A remarkable increase was found in C_{dl} from 56.08 to 556 mF cm^{-2} (Fig. 6d), substantiating the increase in ECSA of hybrid catalyst during the cycling activation process. The physical characterizations after running CV for 4000 cycles are shown in Fig. S8, where the XRD and EDS results (Fig. S8a and b) confirm the existence of MoS_2 nanosheets on graphene substrate, maintaining the atomic ratio of Mo and S at 1:2. Moreover, the TEM images (Fig. S8c) exhibit larger interlayer spacings, 8.75 Å for MoS_2 and 4.37 Å for graphene nanosheets. This phenomenon clearly indicates the activation of MoS_2/graphene catalyst by proton intercalation during the cyclic stability test.

In practical applications, water electrolysis cells may operate at relatively high temperature about 50–70°C. Therefore, the stability of as-produced MoS_2/graphene composite was measured by LSVs at in temperature range from 30 to 120°C (Fig. 7a). In addition, i_0 were measured from the corresponding Tafel slopes, which were shown in Fig. S9 and the electrochemical parameters (η_0 and i_0) were summarized in Table S1. The improvement in HER activities was clearly observed with the increase in temperature by decreasing the onset potentials and increasing in exchange current densities. Even at high temperature

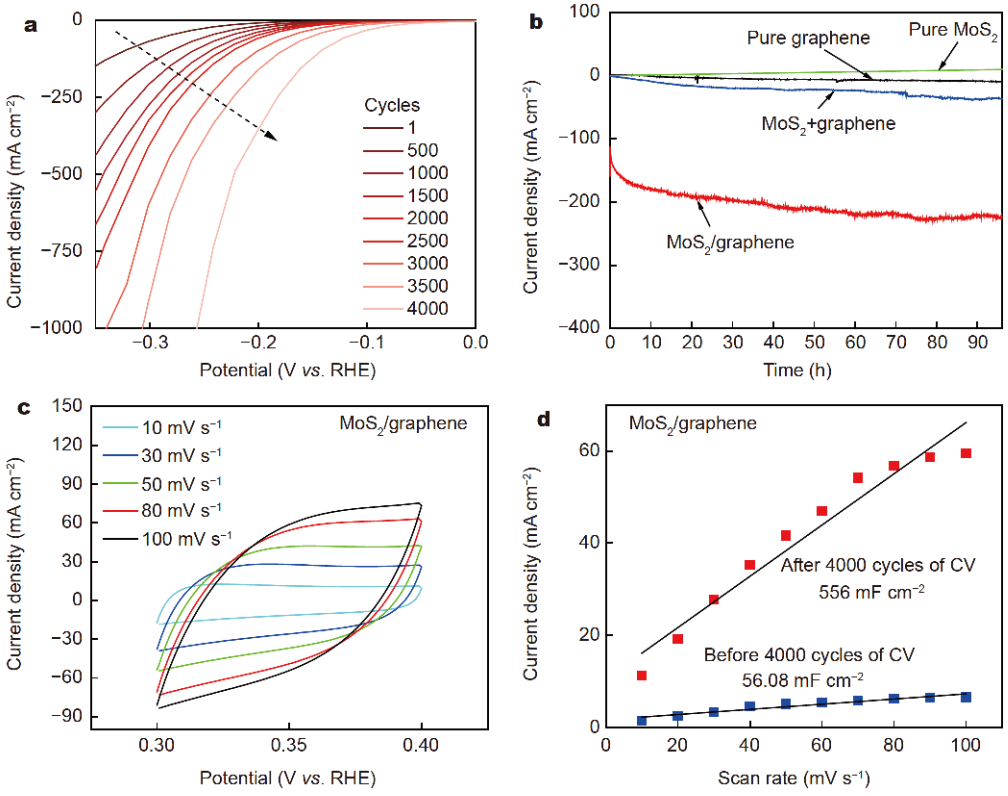

Figure 6 Stability tests with a catalyst load of ~5 mg cm^{-2}: (a) cycling stability of MoS_2/graphene from 0 to −350 mV *vs.* RHE at a scan rate of 50 mV s^{-1} in 0.5 mol L^{-1} H_2SO_4, wherein the polarization curves from 1 to 4000 cycles are displayed; (b) time dependence of cathodic current density on pure MoS_2, graphene, MoS_2+graphene mixture, and MoS_2/graphene composite during electrolysis over 90 h at a constant overpotential of 180 mV; (c) CVs in a potential window without faradaic processes after the 4000 cycles; (d) double layer capacitance measurements for MoS_2/graphene composite, before and after 4000 cycles of CV.

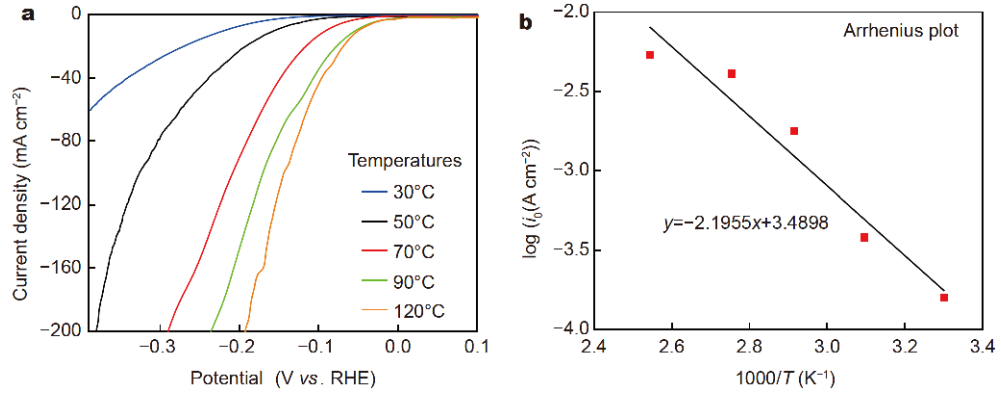

Figure 7 (a) LSVs of MoS_2/graphene composite in a temperature range of 30–120°C in 0.5 mol L^{-1} H_2SO_4, at a scan rate of 1 mV s^{-1}. (b) Corresponding Arrhenius plot for MoS_2/graphene.

of 120°C, MoS_2/graphene shows good stability exhibiting a very low onset potential of 57.2 mV with a high current density. Moreover, activation energy (E_a) is another important parameter to measure the electrocatalytic performance of the HER catalyst. Based on the Arrhenius equation ($k = Ae^{\frac{-E_a}{RT}}$), E_a can be calculated by using the

following Equation (4) [55]:

$$\log(i_0) = \log(A) - \frac{E_a}{2.3RT}, \quad (4)$$

where A is the pre-exponential factor, R is the universal gas constant and T is absolute temperature (in K). Plot of the $\log(i_0)$ as a function of $\frac{1000}{T}$ is shown in Fig. 7b. From the slope of the Arrhenius plot, E_a was calculated to be 36.51 kJ mol^{-1} for MoS_2/graphene-catalyst. This lower activation energy is comparable to Pt catalyst, which displays the E_a in a range of 20–40 kJ mol^{-1} [55,56]. This enhanced catalytic activity and durability indicate that microwave-synthesized MoS_2/graphene nanocomposite is an efficient HER catalyst in acidic medium, even at the higher operating temperatures.

CONCLUSIONS

In conclusion, we have synthesized a highly active electrocatalyst of MoS_2 nanosheets dispersed over graphene by a fast, facile, energy efficient, environmentally friendly route involving reduction of Mo-precursor with presence of CS_2 and graphene under microwave irradiation. Along with being the microwave susceptor, graphene provides a stable conducting network and the large specific surface area for the growth of MoS_2 catalysts, facilitating both the electronic and ion transports between MoS_2/graphene compound and acidic electrolyte, further accelerating the catalytic reaction. As-produced MoS_2/graphene nanocomposite exhibits the enhanced HER activity with a low overpotential and large cathodic current. A small Tafel slope of 43.3 mV/decade suggests a Volmer-Heyrovsky mechanism for the HER. Besides, the catalyst material shows high cycling stability and a continuous hydrogen generation for 90 h at constant potential operation. This non-noble, highly active and stable HER catalyst material is a promising candidate that could accelerate the efforts towards establishing a clean hydrogen-based energy economy. Even though the overpotential (η_{10}) for MoS_2/graphene is higher by 130 mV, it is substantially more preferred for commercial applications than the platinum material since MoS_2 is an earth abundant material and hence much cheaper than Pt. Above all, the microwave-initiated synthesis of MoS_2/graphene nanocomposite *via* an environmentally benign and simple method, capable for extending to large scale, economic production makes it an attractive catalyst for efficient hydrogen generation through water-electrolysis.

Received 15 June 2019; accepted 4 August 2019; published online 29 August 2019

1 Mazloomi K, Gomes C. Hydrogen as an energy carrier: Prospects and challenges. Renew Sustain Energy Rev, 2012, 16: 3024–3033
2 Turner JA. Sustainable hydrogen production. Science, 2004, 305: 972–974
3 Ball M, Wietschel M. The future of hydrogen—opportunities and challenges. Int J Hydrogen Energy, 2009, 34: 615–627
4 Morales-Guio CG, Stern LA, Hu X. Nanostructured hydrotreating catalysts for electrochemical hydrogen evolution. Chem Soc Rev, 2014, 43: 6555
5 Thoi VS, Sun Y, Long JR, *et al.* Complexes of earth-abundant metals for catalytic electrochemical hydrogen generation under aqueous conditions. Chem Soc Rev, 2013, 42: 2388–2400
6 Zou X, Zhang Y. Noble metal-free hydrogen evolution catalysts for water splitting. Chem Soc Rev, 2015, 44: 5148–5180
7 Marinović V, Stevanović J, Jugović B, *et al.* Hydrogen evolution on Ni/WC composite coatings. J Appl Electrochem, 2006, 36: 1005–1009
8 Krstajic N, Jovic V, Gajickrstajic L, *et al.* Electrodeposition of Ni–Mo alloy coatings and their characterization as cathodes for hydrogen evolution in sodium hydroxide solution. Int J Hydrogen Energy, 2008, 33: 3676–3687
9 Han Q. Hydrogen evolution reaction on amorphous Ni–S–Co alloy in alkaline medium. Int J Hydrogen Energy, 2003, 28: 1345–1352
10 Evans DJ, Pickett CJ. Chemistry and the hydrogenases. Chem Soc Rev, 2003, 32: 268
11 Rees DC, Howard JB. The interface between the biological and inorganic worlds: Iron-sulfur metalloclusters. Science, 2003, 300: 929–931
12 Morales-Guio CG, Hu X. Amorphous molybdenum sulfides as hydrogen evolution catalysts. Acc Chem Res, 2014, 47: 2671–2681
13 Yan Y, Xia BY, Xu Z, *et al.* Recent development of molybdenum sulfides as advanced electrocatalysts for hydrogen evolution reaction. ACS Catal, 2014, 4: 1693–1705
14 Laursen AB, Kegnæs S, Dahl S, *et al.* Molybdenum sulfides—efficient and viable materials for electro- and photoelectrocatalytic hydrogen evolution. Energy Environ Sci, 2012, 5: 5577
15 Benck JD, Chen Z, Kuritzky LY, *et al.* Amorphous molybdenum sulfide catalysts for electrochemical hydrogen production: Insights into the origin of their catalytic activity. ACS Catal, 2012, 2: 1916–1923
16 Jaramillo TF, Jørgensen KP, Bonde J, *et al.* Identification of active edge sites for electrochemical H_2 evolution from MoS_2 nanocatalysts. Science, 2007, 317: 100–102
17 Kong D, Wang H, Cha JJ, *et al.* Synthesis of MoS_2 and $MoSe_2$ films with vertically aligned layers. Nano Lett, 2013, 13: 1341–1347
18 Li Y, Wang H, Xie L, *et al.* MoS_2 nanoparticles grown on graphene: An advanced catalyst for the hydrogen evolution reaction. J Am Chem Soc, 2011, 133: 7296–7299
19 Yang Y, Fei H, Ruan G, *et al.* Edge-oriented MoS_2 nanoporous films as flexible electrodes for hydrogen evolution reactions and supercapacitor devices. Adv Mater, 2014, 26: 8163–8168
20 Voiry D, Salehi M, Silva R, *et al.* Conducting MoS_2 nanosheets as catalysts for hydrogen evolution reaction. Nano Lett, 2013, 13: 6222–6227
21 Deng J, Li H, Xiao J, *et al.* Triggering the electrocatalytic hydrogen evolution activity of the inert two-dimensional MoS_2 surface *via* single-atom metal doping. Energy Environ Sci, 2015, 8: 1594–1601
22 Wang H, Lu Z, Xu S, *et al.* Electrochemical tuning of vertically

aligned MoS_2 nanofilms and its application in improving hydrogen evolution reaction. Proc Natl Acad Sci USA, 2013, 110: 19701–19706
23 Gao MR, Liang JX, Zheng YR, *et al.* An efficient molybdenum disulfide/cobalt diselenide hybrid catalyst for electrochemical hydrogen generation. Nat Commun, 2015, 6: 5982
24 Zhu Y, Murali S, Cai W, *et al.* Graphene and graphene oxide: Synthesis, properties, and applications. Adv Mater, 2010, 22: 3906–3924
25 Xiang Q, Yu J, Jaroniec M. Graphene-based semiconductor photocatalysts. Chem Soc Rev, 2012, 41: 782–796
26 Firmiano EGS, Cordeiro MAL, Rabelo AC, *et al.* Graphene oxide as a highly selective substrate to synthesize a layered MoS_2 hybrid electrocatalyst. Chem Commun, 2012, 48: 7687
27 Tang YJ, Wang Y, Wang XL, *et al.* Molybdenum disulfide/nitrogen-doped reduced graphene oxide nanocomposite with enlarged interlayer spacing for electrocatalytic hydrogen evolution. Adv Energy Mater, 2016, 6: 1600116
28 Sun Y, Hu X, Luo W, *et al.* Self-assembled hierarchical MoO_2/graphene nanoarchitectures and their application as a high-performance anode material for lithium-ion batteries. ACS Nano, 2011, 5: 7100–7107
29 Bhaskar A, Deepa M, Rao TN, *et al.* Enhanced nanoscale conduction capability of a MoO_2/graphene composite for high performance anodes in lithium ion batteries. J Power Sources, 2012, 216: 169–178
30 Zhao Y, Xie X, Zhang J, *et al.* MoS_2 nanosheets supported on 3D graphene aerogel as a highly efficient catalyst for hydrogen evolution. Chem Eur J, 2015, 21: 15908–15913
31 Murugesan S, Kearns P, Stevenson KJ. Electrochemical deposition of germanium sulfide from room-temperature ionic liquids and subsequent Ag doping in an aqueous solution. Langmuir, 2012, 28: 5513–5517
32 Jiang Y, Zhu YJ. Microwave-assisted synthesis of sulfide M_2S_3 (M = Bi, Sb) nanorods using an ionic liquid. J Phys Chem B, 2005, 109: 4361–4364
33 Zhang X, Liu Z. Recent advances in microwave initiated synthesis of nanocarbon materials. Nanoscale, 2012, 4: 707–714
34 Liu Z, Zhang L, Poyraz S, *et al.* An ultrafast microwave approach towards multi-component and multi-dimensional nanomaterials. RSC Adv, 2014, 4: 9308
35 Anantharaj S, Kennedy J, Kundu S. Microwave-initiated facile formation of Ni_3Se_4 nanoassemblies for enhanced and stable water splitting in neutral and alkaline media. ACS Appl Mater Interfaces, 2017, 9: 8714–8728
36 Dong GH, Zhu YJ, Chen LD. Microwave-assisted rapid synthesis of Sb_2Te_3 nanosheets and thermoelectric properties of bulk samples prepared by spark plasma sintering. J Mater Chem, 2010, 20: 1976
37 Zhang Y, Qiao ZP, Chen XM. Microwave-assisted elemental direct reaction route to nanocrystalline copper chalcogenides CuSe and Cu_2Te. J Mater Chem, 2002, 12: 2747–2748
38 Liu Z, Zhang L, Wang R, *et al.* Ultrafast microwave nano-manufacturing of fullerene-like metal chalcogenides. Sci Rep, 2016, 6: 22503
39 Li H, Zhang Q, Yap CCR, *et al.* From bulk to monolayer MoS_2: Evolution of Raman scattering. Adv Funct Mater, 2012, 22: 1385–1390
40 Zhang X, Meng F, Mao S, *et al.* Amorphous MoS_xCl_y electrocatalyst supported by vertical graphene for efficient electrochemical and photoelectrochemical hydrogen generation. Energy Environ Sci, 2015, 8: 862–868
41 Lee C, Yan H, Brus LE, *et al.* Anomalous lattice vibrations of single- and few-layer MoS_2. ACS Nano, 2010, 4: 2695–2700
42 Mandal M, Ghosh D, Kalra SS, Das CK. High performance supercapacitor electrode material based on flower like MoS_2/reduced graphene oxide nanocomposite. Int J Latest Res Technol, 2014, 3: 65–69
43 Khan M, Yousaf AB, Chen M, *et al.* Molybdenum sulfide/graphene-carbon nanotube nanocomposite material for electrocatalytic applications in hydrogen evolution reactions. Nano Res, 2016, 9: 837–848
44 Liu Y, Zhao Y, Jiao L, *et al.* A graphene-like MoS_2/graphene nanocomposite as a highperformance anode for lithium ion batteries. J Mater Chem A, 2014, 2: 13109–13115
45 Sheng W, Gasteiger HA, Shao-Horn Y. Hydrogen oxidation and evolution reaction kinetics on platinum: Acid *vs* alkaline electrolytes. J Electrochem Soc, 2010, 157: B1529
46 Thomas JGN. Kinetics of electrolytic hydrogen evolution and the adsorption of hydrogen by metals. Trans Faraday Soc, 1961, 57: 1603–1611
47 Huang Z, Luo W, Ma L, *et al.* Dimeric $[Mo_2S_{12}]^{2-}$ cluster: A molecular analogue of MoS_2 edges for superior hydrogen-evolution electrocatalysis. Angew Chem Int Ed, 2015, 54: 15181–15185
48 Kong D, Wang H, Lu Z, *et al.* $CoSe_2$ nanoparticles grown on carbon fiber paper: An efficient and stable electrocatalyst for hydrogen evolution reaction. J Am Chem Soc, 2014, 136: 4897–4900
49 Tang YJ, Gao MR, Liu CH, *et al.* Porous molybdenum-based hybrid catalysts for highly efficient hydrogen evolution. Angew Chem Int Ed, 2015, 54: 12928–12932
50 McCrory CCL, Jung S, Ferrer IM, *et al.* Benchmarking hydrogen evolving reaction and oxygen evolving reaction electrocatalysts for solar water splitting devices. J Am Chem Soc, 2015, 137: 4347–4357
51 Liao L, Zhu J, Bian X, *et al.* MoS_2 formed on mesoporous graphene as a highly active catalyst for hydrogen evolution. Adv Funct Mater, 2013, 23: 5326–5333
52 Zheng X, Xu J, Yan K, *et al.* Space-confined growth of MoS_2 nanosheets within graphite: The layered hybrid of MoS_2 and graphene as an active catalyst for hydrogen evolution reaction. Chem Mater, 2014, 26: 2344–2353
53 Li G, Zhang D, Yu Y, *et al.* Activating MoS_2 for pH-universal hydrogen evolution catalysis. J Am Chem Soc, 2017, 139: 16194–16200
54 Liu Y, Wu J, Hackenberg KP, *et al.* Self-optimizing, highly surface-active layered metal dichalcogenide catalysts for hydrogen evolution. Nat Energy, 2017, 2: 17127
55 Santos DMF, Sequeira CAC, Macciò D, *et al.* Platinum–rare earth electrodes for hydrogen evolution in alkaline water electrolysis. Int J Hydrogen Energy, 2013, 38: 3137–3145
56 Durst J, Simon C, Hasché F, *et al.* Hydrogen oxidation and evolution reaction kinetics on carbon supported Pt, Ir, Rh, and Pd electrocatalysts in acidic media. J Electrochem Soc, 2014, 162: F190–F203

Acknowledgements This work was supported by Auburn University-Intramural Grants Program (AU-IGP). Authors would like to thank Ali Rashti and Tae-Sik Oh for their help with BET analysis. Authors also thank Horyun Lee for the help with Raman analysis.

Author contributions Sarwar S performed the electrochemical characterizations, analyzed the data and wrote this paper with the input

from all authors. Nautiyal A and Cook J helped with useful suggestions and guidance. Li J and Wang R contributed with SEM and EDS tests. Uprety S and Park M helped with the collection of Raman data and Bozack MJ contributed with XPS tests. Yuan Y and Yassar R were involved with TEM tests and revised the manuscript. Zhang X supervised the entire project and revised the manuscript.

Conflict of interest The authors declare no conflict of interest.

Supplementary information Supporting data are available in the online version of the paper.

Shatila Sarwar received her BSc degree in chemical engineering at Bangladesh University of Engineering & Technology (BUET). She is now a PhD candidate in Prof. Xinyu Zhang's Laboratory at the Department of Chemical Engineering, Auburn University, USA. Her current research focuses on the microwave-initiated synthesis of transition metal dichalcogenides for electrochemical energy conversion and storage applications.

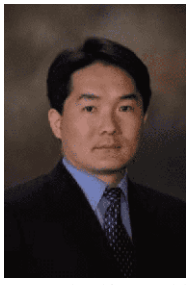

Xinyu Zhang studied in Chemistry Department at the University of Texas at Dallas (UTD) under the supervision of Professors Alan G. MacDiarmid and Sanjeev K. Manohar. After receiving his PhD degree in 2005, he started his postdoctoral stay at the University of Massachusetts Lowell. He started his career at Auburn University in 2008 in the Department of Polymer and Fiber Engineering. His research interests include the microwave approach to ultrafast production of nanomaterials, mechanism study of polymeric material self-assembly using nano-seeding approach, chemical/electrochemical sensors, and polymer-metal nanocomposites. Currently, he is an Associate Professor in the Department of Chemical Engineering, Auburn University.

基于简易微波方法制备高性能MoS_2/石墨烯纳米复合材料用于高效析氢反应

Shatila Sarwar[1], Amit Nautiyal[1], Jonathan Cook[1], 袁一斐[2,3], 李俊豪[4], Sunil Uprety[4], Reza Shahbazian-Yassar[2], 王瑞刚[4], Minseo Park[5], Michael J. Bozack[5], 张新宇[1*]

摘要 用于析氢反应(HER)的低成本、高效能催化剂对于推进基于清洁氢气的能源工业非常重要. 二维二硫化钼(MoS_2)具有显著的催化性能, 因而已被人们广泛深入研究. 然而, 大多数现有的合成方法耗时、复杂且效率较低. 本文通过超快(60秒)微波引发的方法生产MoS_2/石墨烯催化剂. 石墨烯的高比表面积和导电性为MoS_2纳米片的生长提供了有利的导电网络和快速电荷转移动力. 文中制备的MoS_2/石墨烯纳米复合材料在酸性介质中对HER表现出优异的电催化活性, 具有62 mV的低起始电位, 高阴极电流和43.3mV/dec的Tafel斜率. 除了优异的催化活性外, MoS_2/石墨烯还具有较长的循环稳定性, 在250 mV的过电位下阴极电流密度高达1000 mA cm^{-2}. 此外, MoS_2/石墨烯催化剂在30–120°C范围内具有出色的HER活性和36.51 kJ mol^{-1}的低活化能, 提供了潜在的大批量生产和制备的机会.

